Evolution of density-modulated electron beams in drift sections

Shaukat Khan [*]
Center for Synchrotron Radiation and Department of Physics, TU Dortmund University, Maria-Goeppert-Mayer-Str. 2, 44227 Dortmund, Germany

Giovanni Perosa,[†] Filippo Sottocorona,[‡] Alexander Brynes, Giovanni De Ninno,[§] Giuseppe Penco, Primož Rebernic Ribič, Simone Spampinati,[‖] Carlo Spezzani, Mauro Trovò, Luca Giannessi,[¶] and Enrico Allaria
Elettra-Sincrotrone Trieste S.C.p.A., Strada Statale 14—km 163.5 in AREA Science Park, 34149 Basovizza, Italia

Evgeny Schneidmiller and Eugenio Ferrari
Deutsches Elektronen-Synchrotron (DESY), Notkestraße 85, 22607 Hamburg, Germany

(Received 10 December 2023; accepted 6 March 2024; published 26 April 2024)

Initiating the amplification process in a short-wavelength free-electron laser (FEL) by external seed laser pulses results in radiation with a high degree of longitudinal and transverse coherence. The basic layout in seeded harmonic generation involves a periodic electron energy modulation by laser-electron interaction in a short undulator (the "modulator"), which is converted into a density modulation in a dispersive section immediately followed by a long FEL undulator (the "radiator") tuned to a harmonic of the seed laser wavelength. With the advent of more complex seeding schemes, density-modulated beams may need to be transported in drift sections before entering the radiator. Long FEL undulators may also contain several drift spaces to accommodate focusing elements and diagnostics. Therefore, it is of general interest to study the evolution of density-modulated electron beams in drift sections under the influence of repulsive Coulomb forces. At FERMI, a seeded FEL user facility in Trieste, Italy, systematic studies of the impact of varying drift length on coherent harmonic emission were undertaken. In order to make the underlying physics transparent, the emphasis of this paper is on reproducing the experimental findings with analytical estimates and a simple one-dimensional numerical model. Furthermore, the Coulomb forces in a drift section may be employed to enhance the laser-induced energy modulation and yield an improved density modulation before entering the FEL radiator.

DOI: 10.1103/PhysRevAccelBeams.27.040702

I. INTRODUCTION

With unprecedented brightness and femtosecond pulse duration, high-gain free-electron lasers (FELs) in the extreme ultraviolet and X-ray regime have significantly extended the range of scientific opportunities compared to conventional synchrotron light sources [1].

High-gain FELs are based on relativistic electrons from a linear accelerator developing an instability during a single pass in a long undulator magnet [2,3]. The electrons emit radiation which acts back on them causing a periodic modulation of the electron density which, in turn, gives rise to coherent emission of radiation further enhancing the modulation. This process amplifies the radiation field exponentially within a narrow bandwidth around the central wavelength λ given by the undulator period λ_U, the undulator parameter K, and the Lorentz factor γ of the electrons:

$$\lambda = \frac{\lambda_U}{2\gamma^2}\left(1+\frac{K^2}{2}\right) \quad \text{with} \quad K = \frac{eB_0\lambda_U}{2\pi m_e c}, \qquad \gamma = \frac{E}{m_e c^2}. \tag{1}$$

Here, B_0 is the amplitude of the sinusoidal magnetic field along the undulator, E is the electron energy, c is the velocity

[*]shaukat.khan@tu-dortmund.de
[†]Present address: Department of Physics and Astronomy, Uppsala University, Regementsvägen 1, 75237 Uppsala, Sweden.
[‡]Also at Dipartimento di Fisica, Università degli Studi di Trieste, Piazzale Europa 1, 34127 Trieste, Italy.
[§]Also at Laboratory of Quantum Optics, University of Nova Gorica, Vipavska 11c, 5270 Nova Ajdovščina, Slovenia.
[‖]Present address: INFN, Laboratori Nazionali di Frascati, Via Enrico Fermi 54, 00044 Frascati, Italy.
[¶]Also at INFN, Laboratori Nazionali di Frascati, Via Enrico Fermi 54, 00044 Frascati, Italy.

of light, e is the elementary charge, and m_e is the electron rest mass.

For brevity and as elsewhere in the literature (e.g., [2]), the individual maxima of the modulated electron density with periodicity λ will be called "microbunches" in contrast to the whole electron bunch with a typical length in the range of 10 to 100 μm. The formation of microbunches may be initiated by the shot noise of the electrons in the self-amplified spontaneous emission process [3,4] or by "seeding" with an external radiation pulse. In the latter case, the longitudinal coherence of the FEL pulses is greatly improved, and pulse-to-pulse fluctuations of output energy, arrival time, and central wavelength are reduced.

A well-established seeding scheme is high-gain harmonic generation (HGHG) [5,6], where the interaction with laser pulses in an undulator (the "modulator") tuned to the laser wavelength λ_L results in a sinusoidal modulation of the electron energy. In a dispersive section, often a so-called chicane composed of four dipole magnets, the longitudinal electron position in a comoving frame changes by $\Delta z = R_{56} \cdot \Delta E/E$ proportional to the energy offset ΔE and the transfer matrix element R_{56} representing the longitudinal dispersion. In the subsequent FEL undulator (the "radiator"), the resulting microbunches with an equal spacing of λ_L give rise to coherent emission of radiation at harmonics λ_L/h of the laser wavelength, where the harmonic number h is an integer.

The electron density modulation is quantified by the harmonic content of the normalized longitudinal electron density $\rho_e(z)$ with $\int_{-\infty}^{\infty} \rho_e(z) dz = 1$ given by Fourier coefficients

$$b_h = \frac{1}{\lambda_L} \int_0^{\lambda_L} \rho_e(z) \, \exp\left(-i2\pi \frac{hz}{\lambda_L}\right) dz. \tag{2}$$

The absolute value $|b_h|$ is commonly known as the bunching factor of the hth laser harmonic and the power of coherently emitted radiation scales with $|b_h|^2$. In HGHG, the bunching factor can be expressed as [6]

$$|b_h| = \exp\left(-\frac{1}{2} h^2 B^2\right) J_h\,(hAB) \tag{3}$$

with J_h being the hth-order Bessel function of the first kind. With the root-mean-square slice energy spread σ_E, $A = \Delta E/\sigma_E$ is the relative energy modulation amplitude and $B = (2\pi/\lambda_L)(\sigma_E/E)R_{56}$ is the dimensionless longitudinal dispersion. For σ_E/E of the order of 10^{-5}, the FEL gain drops strongly beyond $h \approx 15$ [7]. More complex seeding schemes have been designed to reach higher harmonics. One option is to use two successive HGHG stages while delaying the electrons by a chicane between them. In this "fresh-bunch" scheme (HGHG-FB) [8], a pulse emitted by one part of the electron bunch in the first radiator acts as a seed on a different part of the bunch in the second modulator. In 2009, echo-enabled harmonic generation (EEHG) was proposed [9,10] employing a twofold laser-electron interaction and two dispersive sections to generate a complex electron density distribution with high harmonic content. With $|b_h| \propto h^{-1/3}$, much higher harmonics can be reached compared to single-stage HGHG, as has been demonstrated experimentally [11,12].

FEL facilities with multiple undulators and dispersive sections offer the possibility to switch between HGHG and a more complex seeding scheme depending on the wavelength and other requirements of the respective scientific application. Here, the electron beam may need to be transported from the dispersive section to the FEL radiator along extended drift sections. Furthermore, long radiators may contain drift spaces that are required to accommodate focusing and orbit-correcting magnets, beam position monitors, and other diagnostics elements. Therefore, the aim of the study presented here is to understand the evolution of density-modulated electrons in a drift section under the influence of repulsive Coulomb forces between them. It is expected that the strongly increased charge density of the microbunches gives rise to a significant longitudinal space-charge (LSC) effect within a few meters of drift space. LSC increases the energy spread within the microbunches causing a nonlinear longitudinal elongation ("debunching"). On the other hand, the correlated energy spread (i.e., the energy offset of electrons between the microbunches as function of z) can be reduced. This was proposed as a way to improve the output of HGHG FELs [13].

The experimental studies partly presented in [14,15] and discussed below were performed at the FERMI user facility [16] of the Elettra laboratory located in Trieste, Italy. FERMI produces powerful radiation in the spectral range from 100 to 4 nm with two seeded FEL lines, FEL-1 and FEL-2. Both provide a high degree of longitudinal and transverse coherence enabling experiments not possible with other radiation sources. Until recently, FEL-1 [17] was based on single-stage HGHG with a radiator composed of six undulators as shown in Fig. 1. In order to extend its spectral range, FEL-1 was recently upgraded to implement the EEHG scheme [18] which was before demonstrated at FEL-2 [12]. In routine operation, the FEL-2 beamline [19]

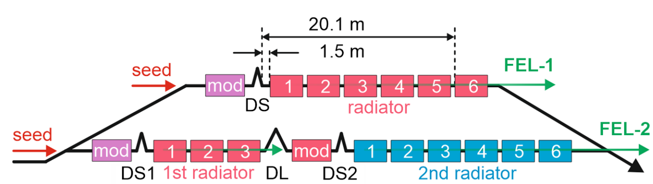

FIG. 1. Schematic view of the seeded FEL lines of FERMI as of 2022 with modulators (mod), radiators, dispersive sections (DS), and a delay line (DL) for two-staged HGHG. Also indicated is the shortest and longest drift length between DS and a radiator in FEL-1 (not to scale, see also Table 1).

employs the HGHG-FB scheme [8] based on two successive modulator-radiator stages. As a future upgrade, a combination of EEHG with an HGHG-FB stage is being considered [20].

II. ANALYTICAL ESTIMATES

A laser-induced sinusoidal modulation of the electron energy followed by a dispersive section with an appropriate longitudinal dispersion R_{56} leads to a tilted sinusoidal phase space distribution with sharp density maxima along the longitudinal z axis in a comoving frame as shown in the top part of Fig. 2. Electrons preceding these microbunches have negative, trailing electrons have positive energy offset. The drift length over which the LSC force significantly impairs the coherent emission of radiation at harmonic h of a seed laser wavelength λ_L can be estimated by the following considerations resulting in a simple formula.

As also shown in Fig. 2, the microbunches may be modeled as disks with length σ_z, area a, and charge $Q < 0$ causing a longitudinal electric field $\mathcal{E}$. According to the usual sign convention, the electric field points toward the disks, and the repulsive LSC force tends to increase their length. The dilute electrons between the microbunches form an almost homogeneous line charge with a radial field, which is ignored in the following. Application of Gauss's law yields

$$\mathcal{E} = \frac{Q}{2a\varepsilon_0} = \frac{I}{2\pi\varepsilon_0 c k_L \sigma_{x,y}^2}, \tag{4}$$

where ε_0 is the vacuum permittivity, $k_L = 2\pi/\lambda_L$ is the laser wave number, and I is the electron current before passing the dispersive section. The microbunch charge is estimated to be $Q = I\lambda_L/(2\pi c) = I/(ck_L)$, i.e., a longitudinal fraction $1/(2\pi)$ of the initially homogeneous charge. The transverse area is assumed to be $a = \pi\sigma_{x,y}^2$ with the root-mean-square size $\sigma_{x,y}$ of a round beam.

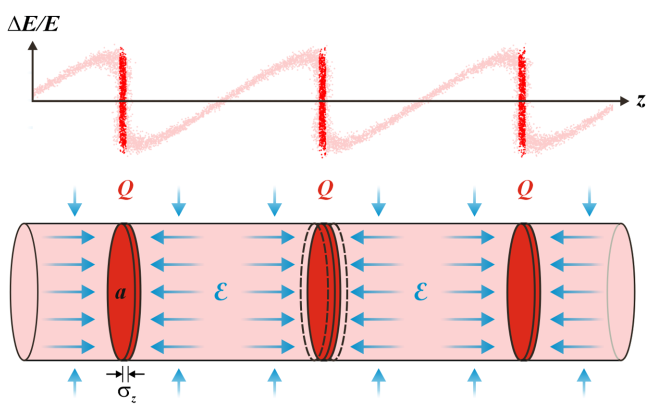

FIG. 2. Top: electrons in longitudinal phase space after energy modulation followed by a dispersive section. Bottom: model of microbunches with charge $Q < 0$ as disks (red) with area a and thickness σ_z. The electric field $\mathcal{E}$ perpendicular to a short cylindrical box surrounding charge Q (dashed lines) is given by Gauss's law: $2a \cdot \mathcal{E} = Q/\varepsilon_0$. The electric field of the almost homogeneous dilute charge between the microbunches (light red) is predominantly radial.

As function of the longitudinal position s after the dispersive section, the repulsive force causes a difference of the Lorentz factor at either end of the microbunch given by

$$\Delta\gamma(s) = \frac{e\mathcal{E}}{m_e c^2} s. \tag{5}$$

With $\beta \approx 1 - 1/(2\gamma^2)$, the resulting velocity mismatch is

$$\Delta\beta(s) = \frac{1}{2\gamma^2} - \frac{1}{2[\gamma + \Delta\gamma(s)]^2} \approx \frac{\Delta\gamma(s)}{\gamma^3}. \tag{6}$$

If, however, the microbunches travel along an undulator with strength parameter K, the average electron velocity is reduced to $\beta \approx 1 - (1 + K^2/2)/(2\gamma^2)$ and Eq. (6) is modified to

$$\Delta\beta(s) = \left(1 + \frac{K^2}{2}\right)\frac{\Delta\gamma(s)}{\gamma^3} = \frac{\Delta\gamma(s)}{\gamma\gamma_r^2}, \tag{7}$$

where $\gamma_r = \gamma/\sqrt{1 + K^2/2}$ is the reduced Lorentz factor. In order not to influence the FEL radiation output, an undulator acting as drift space with reduced Lorentz factor should be tuned away from the seed harmonics. Over a distance L, the microbunch is lengthened by

$$\begin{aligned} \Delta z &= \int_0^L \Delta\beta(s)ds = \frac{e\mathcal{E}}{m_e c^2 \gamma\gamma_r^2}\frac{L^2}{2} \\ &= \frac{eIL^2}{4\pi\varepsilon_0 k_L m_e c^3 \sigma_{x,y}^2 \gamma\gamma_r^2} = \frac{IL^2}{I_A k_L \sigma_{x,y}^2 \gamma\gamma_r^2}, \end{aligned} \tag{8}$$

where $I_A \equiv 4\pi\varepsilon_0 m_e c^3/e \approx 17$ kA is the Alfvén current. The broadening of an initially very short microbunch is considered to be significant when its length reaches

$$\Delta z \approx \frac{\lambda_L}{2\pi h} = \frac{1}{k_L h} \tag{9}$$

and by comparison with Eq. (8), the final expression

$$L \approx \sigma_{x,y}\gamma_r \sqrt{\frac{\gamma I_A}{hI}} \tag{10}$$

is obtained. This order-of-magnitude estimate of the characteristic debunching distance L depends on electron current I, transverse size $\sigma_{x,y}$, and Lorentz factor γ, while the retarding effect of a detuned undulator is included by γ_r. Equation (10) is based on the assumption of a purely longitudinal electric field which is valid for disklike microbunches with $\sigma_x \gg \sigma_z \cdot \gamma_r$ [3]. Note that it does not depend on the laser-induced modulation amplitude A because the A-dependent finite length of the microbunch directly after the dispersive section was neglected.

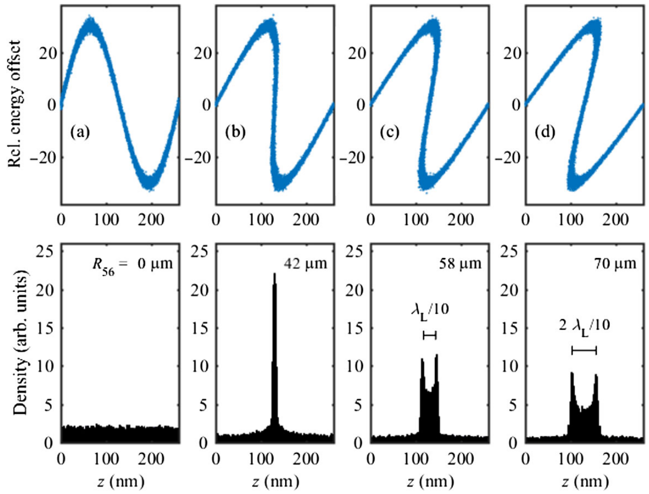

FIG. 3. Relative energy offset in units of σ_E (top) and electron density (bottom) as function of the longitudinal coordinate z over one laser wavelength (here: $\lambda_L = 260$ nm) after energy modulation with amplitude $\Delta E/\sigma_E = 26$ and sections with different longitudinal dispersion: (a) $R_{56} = 0$ µm; (b) $R_{56} = 42$ µm, optimum density modulation; (c) $R_{56} = 58$ µm, density modulation with two peaks $\lambda_L/10$ apart; (d) $R_{56} = 70$ µm, density modulation with two peaks $2\lambda_L/10$ apart. Cases (b)–(d) give rise to the first three maxima of bunching factor $|b_{10}|$ as function of R_{56}.

III. NUMERICAL SIMULATIONS

An optimized dispersive section results in a phase space distribution as shown in Figs. 2 and 3(b). Increasing R_{56} further causes a double peak of the electron density. Additional maxima of the bunching factor $|b_h|$ at the hth seed harmonic are obtained when the peaks are an integer multiple of λ_L/h apart as in Figs. 3(c) and 3(d).

In addition to increasing the energy spread within each microbunch, the repulsive LSC forces accelerate the electrons preceding a microbunch and reduce the energy of trailing electrons. If the drift section is long enough, the correlated energy spread of electrons between the microbunches is first minimized and increases thereafter with the opposite sign. This is shown in Fig. 4 using a one-dimensional model, which provides good insight into the process. Following the notation of Ref. [13], the coupled equations

$$\frac{dp_i}{d\tau} = \frac{2}{\alpha}\sum_{h=1}^{\infty} b_h \frac{\sin h\theta_i}{h} \quad \text{and} \quad \frac{d\theta_i}{d\tau} = \alpha p_i \tag{11}$$

are iterated for macroparticles ($i = 1, \ldots n$) in small steps of plasma phase advance τ. The phase space coordinates are $p_i(\tau) = dE_i/\sigma_E$, where the energy offset dE_i is normalized to the energy spread σ_E, and $\theta_i = k_L z_i$ with laser wave number k_L and z_i being the longitudinal coordinate in a comoving frame. The plasma phase advance τ translates into longitudinal position s in the laboratory system via $\tau = k_P\, s$, where

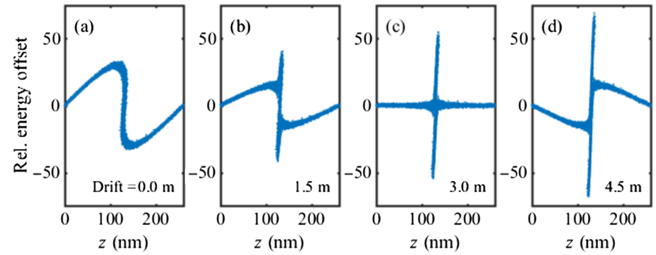

FIG. 4. Relative energy offset in units of σ_E as function of the longitudinal coordinate z over one laser wavelength (here: $\lambda_L = 260$ nm) with increasing drift distance s after density modulation: (a) $s = 0$ m; (b) $s = 1.5$ m, correlated energy spread between the microbunches decreases; (c) $s = 3.0$ m, minimum correlated energy spread; (d) $s = 4.5$ m, overshoot of energy offset between the microbunches. While the energy spread within the microbunch steadily increases with drift distance, the squared bunching factor $|b_{10}|^2$ decreases from 0.078 to 0.068. In this example: electron energy $E = 1300$ MeV, peak current $I = 700$ A, and beam size $\sigma_{x,y} = 60$ µm.

$$k_P = \sqrt{e^2 n_0/m_e c^2 \varepsilon_0 \gamma^3} \tag{12}$$

is the plasma wave number with the electron density n_0, which is assumed here to be constant. Furthermore, the parameter $\alpha \equiv (k_L/k_P)(\sigma_E/E)/\gamma^2$ normalizes the frequency of the plasma oscillation described by Eq. (11). In this model, the bunching factor is obtained by replacing the integral over the charge density in Eq. (2) with a sum over macroparticles

$$|b_h| = \frac{1}{n}\left|\sum_{i=1}^{n} \exp(ih\theta_i)\right|, \tag{13}$$

which has to be updated at every iteration.

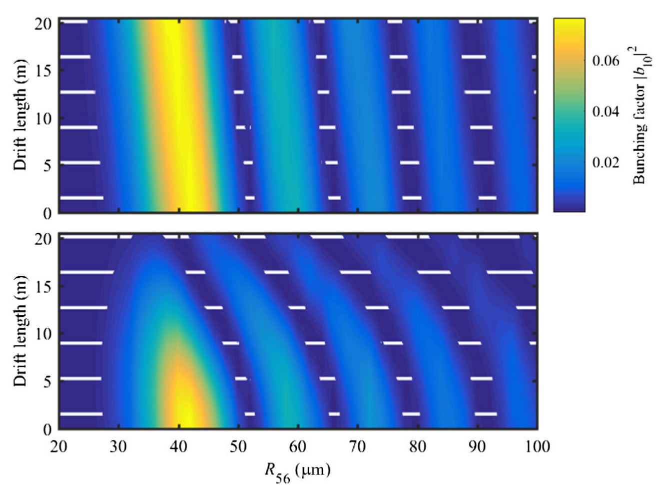

FIG. 5. Color-coded squared bunching factor $|b_{10}|^2$ of the 10th seed harmonic as function of R_{56} and drift length. The white lines correspond to the drift between the dispersive section and the undulators of the FEL-1 beamline. Top: with negligible current, no LSC. Bottom: with a current of 700 A.

The first of the coupled equations (11) describes the change in energy due to a longitudinal electric field caused by a gradient of the charge distribution, which is here assumed to be a periodic function and given by a Fourier sum over harmonics h. The second equation can be rewritten as $dz_i/ds = (dE_i/E)/\gamma^2$ meaning that relativistic particles with an energy offset dE_i change their longitudinal position due to a velocity mismatch.

As function of R_{56} and drift length, Fig. 5 shows the maxima of the squared bunching factor for the 10th seed harmonic as discussed in the context of Fig. 3. For small current and negligible LSC (Fig. 5, top), the maxima are shifted linearly with increasing drift length s, which provides additional longitudinal dispersion $\Delta z/(\Delta\gamma/\gamma) = \Delta\beta s/(\Delta\gamma/\gamma) = s/\gamma^2$ as described by Eq. (6) for the case of constant $\Delta\gamma$. With a moderate current of $I = 700$ A (Fig. 5, bottom), the relationship between Δz and drift length is nonlinear according to Eq. (8), and broadening of the microbunches strongly reduces the bunching factor. From the discussion in Sec. II and Eq. (10), it is obvious that the first maximum decreases faster than the other ones. The first maximum corresponds to a microbunch with charge Q. Since the other maxima are caused by the same charge distributed over two density peaks and the gap between them as shown in Figs. 3(c) and 3(d), their debunching length should be more than a factor of $\sqrt{2}$ longer. Thus, the relative height between the first and the other maxima changes along the drift section.

IV. EXPERIMENTAL SETUP

In contrast to other experimental LSC studies (e.g., [21]), the layout of FERMI shown in Fig. 1 allows to study the evolution of microbunches under variation of the drift length before entering the radiator. With the FEL-1 radiator comprising six individual undulators, using N undulators as radiator simultaneously allows for $7 - N$ different values of drift length. This paper concentrates on configurations with $N = 1$, i.e., a single undulator as radiator preceded by zero to five undulators with detuned magnetic gap. If not specified otherwise, these undulators were fully open (gap 100 mm) and acted as drift spaces. The experimental parameters are summarized in Table I.

TABLE I. Summary of experimental parameters.

Parameter	Value
Beam energy E	1300 MeV
Relative slice energy spread $\sigma_{\Delta E/E}$	2 to 8×10^{-5}
Bunch peak current I	350 to 1400 A
Normalized emittance $\epsilon_{x,y}$	1×10^{-6} m rad
Average beta function $\beta_{x,y}$	10 m
Seed wavelength λ_L	260 nm
Seed pulse energy E_L	24 to 26 μJ
Longitudinal dispersion R_{56}	0 to 100 μm
Drift length s in FEL-1	1.5 to 20.1 m (six steps)

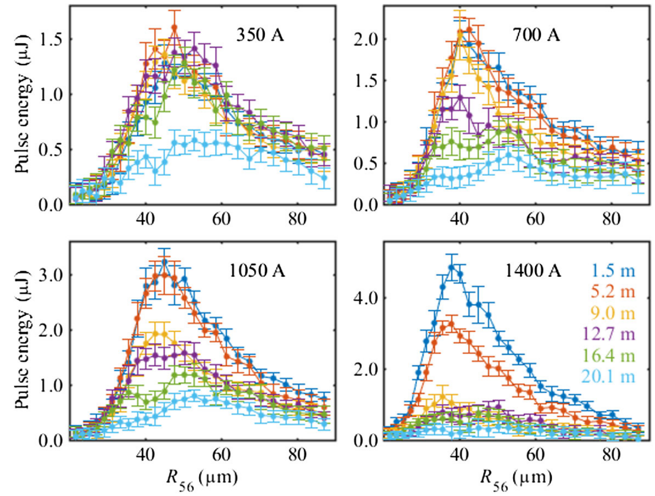

FIG. 6. Measured single-undulator pulse energy at the 10th seed harmonic as function of longitudinal dispersion R_{56} for drift lengths from 1.5 to 20.1 m (radiator 1 to 6) and estimated currents ranging from 350 to 1400 A.

The FEL pulse intensity generated at the 10th harmonic of the laser wavelength was recorded using an intensity monitor (I_0M) based on the photoionization of a low-density rare gas [22]. In addition, a spectrometer (PRESTO) comprising a dispersive grating and a CCD detector [23] could be used to measure the intensity, but the pulse energy from a single undulator turned out to be too low for this instrument.

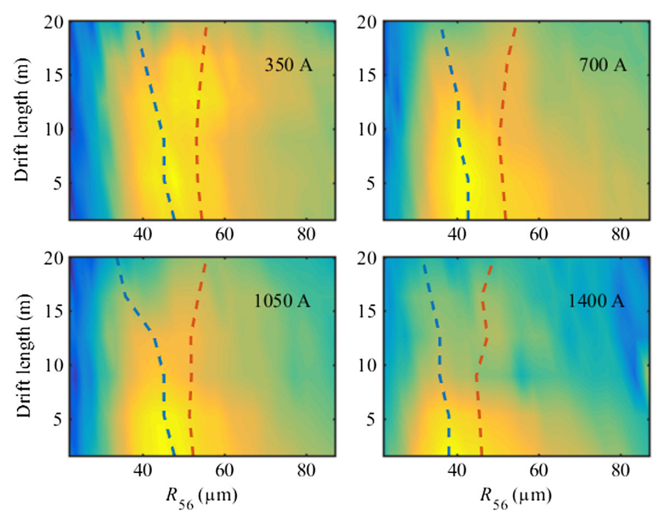

FIG. 7. Color-coded visualization of the pulse energy values shown in Fig. 6 as function of R_{56} and drift length. With increasing drift, the centroid of the intensity distribution over R_{56} (red dashed line) tends toward higher values while the approximate position of the first maximum (blue dashed line) shifts to lower R_{56} consistent with the simulation result shown in Fig. 5.

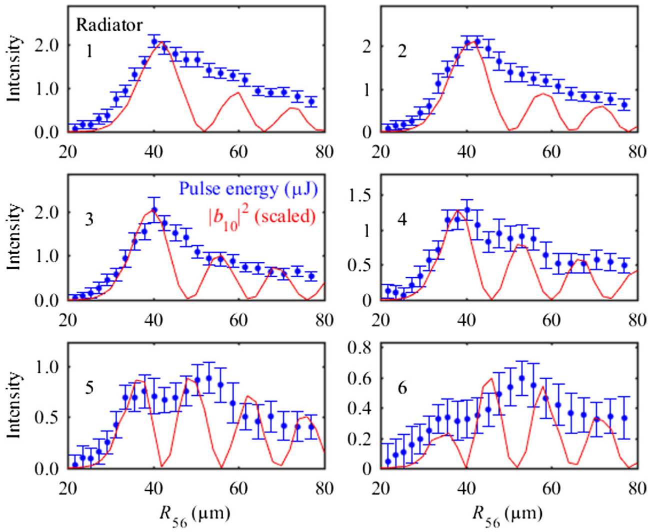

FIG. 8. Intensity in terms of pulse energy from radiator 1 to 6 (blue) and calculated values of $|b_{10}|^2$ (red) as function of R_{56} of the dispersive section for a current of $I = 700$ A. For each radiator, the bunching factor was scaled to the maximum of the measured pulse energy.

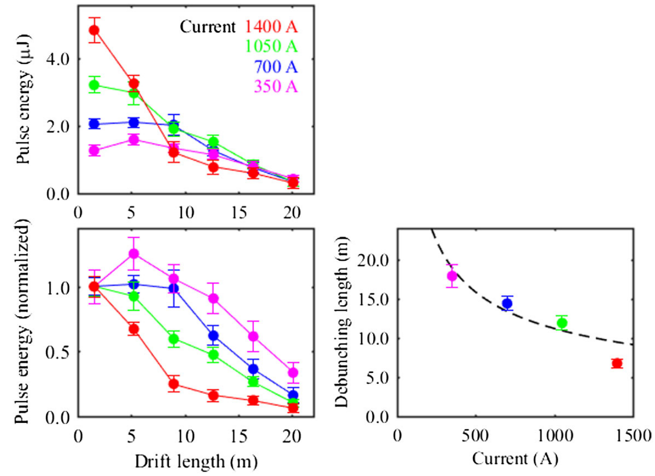

FIG. 9. Left: pulse energy of the respective first maximum of the R_{56} scans in Fig. 6 as function of drift length in μJ (top) and normalized to the value at drift length 1.5 m (bottom). Right: drift length at which the pulse energy reduces by a factor of 2 (interpolated from the left figure) as function of current. Dashed line: debunching length from Eq. (10).

Measurements of the pulse energy were performed under a variation of the R_{56} value of the dispersive section following the modulator. These R_{56} scans were repeated for the six radiator configurations mentioned above and for different electron densities by modifying the bunch compression accordingly. The peak current of the bunches was estimated from radiation coherently emitted by the last magnet of the bunch compressor BC1 and focused onto a pyroelectric detector [24,25]. The slice energy spread is assumed to scale linearly with the current.

V. RESULTS

Figure 6 shows the pulse energy from a single undulator at beamline FEL-1 measured at the 10th harmonic of the seed wavelength of 260 nm while scanning the R_{56} value of the dispersive section (22 to 87 μm), for six different drift lengths (1.5 to 20.1 m for radiator 1 to 6), and for four different values of current (350 to 1400 A). Background radiation from the dispersive section magnets, which shows up with a characteristic R_{56} dependence in the I_0M monitor, was subtracted.

With a radiator length of 2.4 m, the effect of FEL dynamics will be small and the pulse energies can be assumed to be comparable to the squared bunching factors obtained in the simulation. The effect of debunching, i.e., the reduction of pulse energy with drift length, depends strongly on the current, confirming its collective nature. As the drift length increases, the centroid of the intensity distribution tends toward higher R_{56} values as indicated by the red dashed lines in the color-coded representation of the data in Fig. 7. The blue dashed lines indicate the approximate position of the first maximum. With increasing drift length, it shifts to lower R_{56} while the second peak at larger R_{56} becomes more prominent.

The measured pulse energy for the standard current of 700 A and radiator 1 to 6 is shown again in Fig. 8. The red lines represent the simulation result from Fig. 5 for the respective drift lengths. The peak structure of the simulation is barely recognizable in the measured distribution. While the simulation was performed using a uniform modulation amplitude to investigate the LSC effect, the seed laser pulses in the experiment follow longitudinally a normal distribution. Therefore, the maximum energy modulation is accompanied by a tail of lower $\Delta E/E$, which requires larger values of $R_{56} = \Delta z/(\Delta E/E)$ for optimum longitudinal displacement Δz. Thus, the low-R_{56} edges of the observed peaks in Fig. 8 are consistent with the simulation while their slopes toward higher R_{56} are smeared out. In the simulation, the maximum modulation amplitude was adapted to the low-R_{56} edge of the data ($\Delta E/E = 1.05$ to 1.25×10^{-3}). No further adjustment of, e.g., emittance, average beta function, or current was attempted to improve the match. As pointed out before, the initial modulation amplitude does not enter the estimated debunching length in Eq. (10), and repeating the simulation with different modulation amplitudes also shows little effect on the bunching factor as function of drift distance.

As far as the peak structure can be identified in the experimental data, the predicted shift of the peaks toward lower R_{56} with increasing drift length is confirmed. Also visible is the different dependence of the first and the subsequent maxima on drift length as observed in the simulation. While the maxima shift toward lower R_{56}, the debunching effect on the first maximum is stronger than on the others, which causes the centroid of the distribution to shift toward higher R_{56} values.

Figure 9 shows the pulse energy of the first maximum as function of drift length for different electron currents. The interpolated drift length at which the pulse energy reduces by a factor of 2 is shown in the right figure as function of current. The dashed line represents Eq. (10) for $h = 10$, $\sigma_{x,y} = \sqrt{\varepsilon_{x,y}\beta_{x,y}/\gamma} = 67$ μm, and $\gamma_\mathrm{r} = \gamma = 2244$ (see parameters in Table I). The analytical estimate of the debunching length reproduces the right order of magnitude and the dependence on current I. Given the simplicity of the model, however, the very good numerical agreement is certainly a lucky coincidence. Furthermore, the experimental data do not decrease steadily with drift length. Except for high electron density (current 1400 A), the signal at a drift of 5.2 m is comparable or even slightly larger than the value at 1.5 m. Similar observations were made in other experiments with more than one undulator as radiator which are not discussed in this paper. The numerical simulation, which only calculates the bunching factor at the end of the drift section without FEL gain, does not predict this feature. It becomes more pronounced with decreasing current (i.e., increasing debunching length) and may indicate the onset of FEL amplification enhanced by the reduction of correlated energy spread between the microbunches as suggested in [13]. However, it is difficult to firmly rule out experimental uncertainties such as variations of the gain in different radiators due to different optical functions or imperfect electron trajectory. Definite conclusions are subject to further analysis and may require additional measurements, e.g., studying this apparent enhancement at different harmonic numbers.

In a different series of measurements, a single undulator of the FEL-1 beamline was tuned to the 6th seed harmonic and the pulse energy was recorded under variation of the K value of the preceding detuned undulators. Figure 10 shows the results for radiator 2 (left) and radiator 3 (right). Since the debunching length is expected to scale linearly with the reduced Lorentz factor according to Eq. (10), a function $I_0 \times \exp(-d_\mathrm{U}/\gamma_r - d/\gamma)$ was fitted to the data with the zero-K intensity I_0 as a free parameter. Here, d_U is the total length of detuned undulators preceding the radiator, and d represents the combined length of field-free drift spaces between dispersive section and radiator. Since an increasing K value decreases γ_r and shortens the debunching length, the intensity at a fixed distance after the dispersive section is reduced.

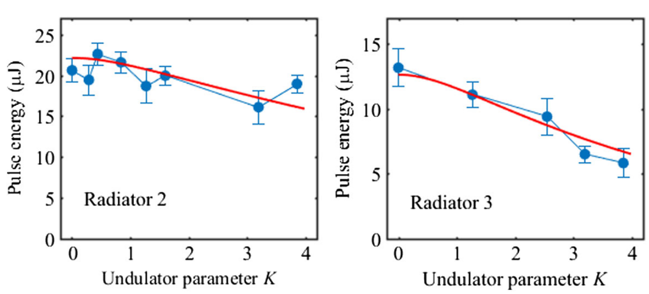

FIG. 10. Pulse energy from radiator 2 (left) and radiator 3 (right) under variation of the K parameter of the preceding undulators. The red lines represent fits to the data points using Eq. (10).

VI. SPACE-CHARGE-ENHANCED MODULATION

The effect of LSC allows to efficiently manipulate the phase space distribution of electrons starting from a rather small laser-induced modulation. In [26], for example, it was proposed to replace the second electron-laser interaction in the EEHG scheme by LSC in a long drift section. In the following, a less elaborate scheme for space-charge-enhanced modulation (SCEM) will be proposed.

Starting from the simulated phase space distribution in Fig. 11(a) directly after laser-induced energy modulation with amplitude $A = \Delta E/\sigma_E = 30$ and a dispersive section DS1, LSC reduces the correlated energy spread of electrons between the microbunches as discussed above. This process continues beyond the point of minimum energy spread shown in Fig. 11(b) leading to a larger energy spread than before with an opposite sign and a quite linear correlation between energy and longitudinal coordinate—see Fig. 11(c). After a second dispersive section DS2, new microbunches are formed from the electrons between the original density maxima as shown in Fig. 11(d). In a second example with lower modulation amplitude ($A = 10$) shown in Figs. 11(e)–11(h), the difference between initial and final energy spread is even larger. The R_{56} value of DS2 has to be

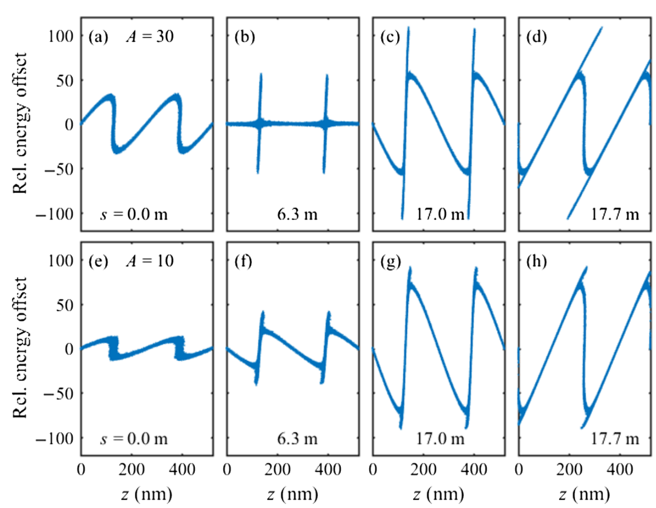

FIG. 11. Two examples of space-charge-enhanced modulation with relative modulation amplitudes $A = 30$ (top row) and $A = 10$ (bottom row). The initial maxima of the electron density are at $z = 130$ and 390 nm. The drift lengths s after the first dispersive section are 0.0 m (a,e), 6.3 m (b,f), and 17.0 m (c,g) followed by a second dispersive section (d,h) resulting in a new density maximum at $z = 260$ nm.

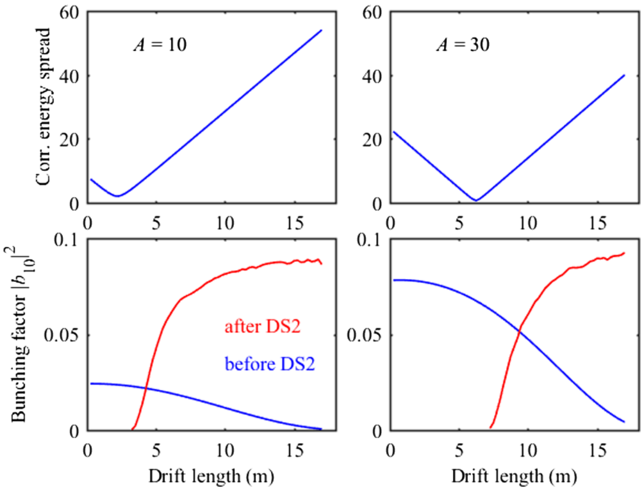

FIG. 12. Top: evolution of correlated energy spread (here: root mean square value of energy offset excluding a region of ± 10 nm around the microbunches) with initial modulation amplitude $A = 10$ (left column) and $A = 30$ (right column). Bottom: squared bunching factor $|b_{10}|^2$ of the 10th seed harmonic before (blue) and after (red) a second dispersive section DS2 as function of drift length between the two dispersive sections.

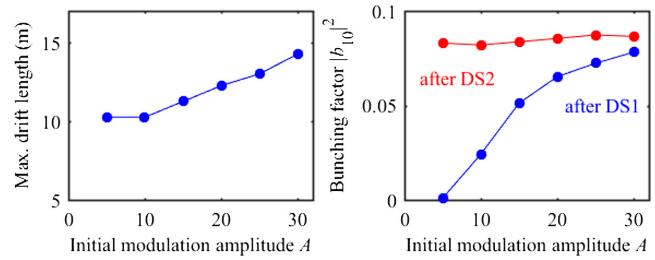

FIG. 13. Left: Maximum drift as function of the initial modulation amplitude A for a correlated energy spread limited to $\sigma_{\Delta E}/\sigma_E \leq 30$. Right: Squared bunching factor after the first dispersive section DS1 (blue) and after DS2 (red) placed at maximum drift according to the left graph.

adapted to the correlated energy spread of the electrons between the initial microbunches in order to optimize the bunching factor. As in the case of DS1, a lower energy spread requires a higher longitudinal dispersion.

The evolution of correlated energy spread between the microbunches is shown in Fig. 12 (top) for two cases, $A = 10$ and 30, illustrating the counterintuitive result that a lower initial modulation amplitude leads to a larger modulation with opposite sign after a given drift length. In other words, a lower initial modulation leads to the same squared bunching factor at a shorter drift, see Fig. 12 (bottom). This is because the energy change per length depends only little on A, as discussed in Sec. II, and a lower correlated energy spread reaches its minimum earlier.

The second dispersive section DS2 may be placed at any position beyond the minimum of the correlated energy spread. The squared bunching factor of the new microbunches rises with drift length and saturates at a value depending only weakly on the initial modulation. Thus, SCEM can be employed to significantly enhance the bunching factor for an initially low modulation. At higher amplitudes, it can be used to recover the initial bunching factor after debunching in a drift space. Similar results are obtained for other seed harmonics.

The calculation was performed for a current of $I = 350$ A and the final bunching factor does not depend significantly on the current except that the evolution happens faster for a higher current. This may be different in a full three-dimensional simulation where space charge also influences the transverse bunch dimensions and thus modifies the electron density n_0 entering Eq. (12). For a given position of DS2, excessive shot-to-shot variations of the current would result in different correlated energy spread, which in combination with a fixed R_{56} value leads to fluctuations of the bunching factor.

While the bunching factor of the new microbunches still rises with drift length, the strongly increasing energy spread may limit the gain of a subsequent FEL. Setting a limit of $\sigma_{\Delta E}/\sigma_E \leq 30$, as an example, yields the maximum drift length shown in Fig. 13 (left) as function of the initial modulation amplitude. With this restriction, the resulting squared bunching factor is still enhanced, especially at low values of A (Fig. 13, right). Therefore, SCEM may be particularly advantageous for seeded FELs with high repetition rate or short seed wavelength, where the seed pulse energy becomes a limiting factor. Of course, a lower modulation amplitude will require a larger R_{56} value at DS1 to obtain the initial microbunches.

The use of LSC to create an energy modulation has already been demonstrated with MeV-scale electron bunches from a photoinjector driven by a laser pulse train [27]. Here, the energy modulation does not change sign but starts from zero under the influence of an initial density modulation, leading to coherent radiation emission in the terahertz regime. Another method to drive a seeded FEL with low-energy laser pulses makes use of an optical klystron configuration preceding the radiator [28,29], where the weak laser-induced modulation in a first undulator is converted to a slight density modulation in a dispersive section followed by self-amplification in a second undulator, both tuned to the seed wavelength.

Both FEL beamlines of FERMI (see Fig. 1) are suited for first experimental tests of SCEM. In the two-stage HGHG configuration of FEL-2, the dispersive section DS1 is followed by a fixed drift length of 17 m before DS2 and the radiator. The radiator of the first stage and the modulator of the second stage would be disabled. The beamline FEL-1 was recently modified for EEHG which includes two modulators, each followed by a dispersive section (not shown in Fig. 1) and a radiator [18]. Compared to FEL-2, this configuration with the second EEHG modulator disabled allows to test SCEM with larger R_{56}

settings of DS1 and shorter drift length. In both cases, the effective drift length between DS1 and DS2 can be increased by tuning the reduced Lorentz factor γ_r with the undulators between the two dispersive sections according to Eq. (10).

VII. CONCLUSIONS

For density-modulated electron beams in seeded FELs, the peak current is high enough to cause LSC-induced debunching along a drift section of only a few meters in length. Measurements at FERMI under variation of drift length, longitudinal dispersion, and electron density are in good qualitative agreement with one-dimensional numerical simulations.

As a general conclusion, the transport of density-modulated beams along long drift spaces should be avoided in the design of FELs with complex seeding schemes, whereas the propagation of a beam without microbunches is not critical. Further investigations will reveal whether and to what degree the reduction of correlated energy spread between the microbunches in a dedicated short drift space could be beneficial for coherent harmonic emission.

In addition to laser-induced energy modulation, the effect of LSC in drift spaces allows to modify the energy of density-modulated electrons and provides an additional handle on the longitudinal phase space distribution. First numerical simulations suggest that an initially small laser-induced energy modulation can be significantly enhanced.

ACKNOWLEDGMENTS

S. K. would like to thank the TU Dortmund University and its Physics Department for granting a sabbatical term. The kind hospitality of the FERMI team and the support during the measurements and data analysis are gratefully acknowledged. The research visit was supported by the Heinrich-Hertz-Stiftung, Ministerium für Kultur und Wissenschaft, NRW, Germany.

[1] *Synchrotron Light Sources and Free-Electron Lasers,* 2nd ed., E. J. Jaeschke, S. Khan, J. R. Schneider, and J. B. Hastings, Springer Reference (Springer, Cham, Switzerland, 2020), 10.1007/978-3-319-14394-1.

[2] P. Schmüser, M. Dohlus, J. Rossbach, and C. Behrens, *Free-Electron Lasers in the Ultraviolet and X-Ray Regime* (Springer, Cham, Switzerland, 2014), 10.1007/978-3-319-04081-3.

[3] E. L. Saldin, E. A. Schneidmiller, and M. V. Yurkov, *The Physics of Free Electron Lasers* (Springer, Heidelberg, Germany, 2000), 10.1007/978-3-662-04066-9.

[4] A. M. Kondratenko and E. L. Saldin, Generation of coherent radiation by a relativistic electron beam in an ondulator, Part. Accel. **10**, 207 (1980).

[5] I. Boscolo and V. Stagno, The converter and the transverse optical klystron, Nuovo Cimento Soc. Ital. Fis. B **58**, 267 (1980).

[6] L. H. Yu, Generation of intense uv radiation by subharmonically seeded single-pass free-electron lasers, Phys. Rev. A **44**, 5178 (1991).

[7] G. Penco, G. Perosa, E. Allaria, S. Di Mitri, E. Ferrari, L. Giannessi, S. Spampinati, C. Spezzani, and M. Veronese, Enhanced seeded free electron laser performance with a "cold" electron beam, Phys. Rev. Accel. Beams **23**, 120704 (2020).

[8] L.-H. Yu and I. Ben-Zvi, High-gain harmonic generation of soft X-rays with the "fresh bunch" technique, Nucl. Instrum. Methods Phys. Res., Sect. A **393**, 96 (1997).

[9] G. Stupakov, Using the beam-echo effect for generation of short-wavelength radiation, Phys. Rev. Lett. **102**, 074801 (2009).

[10] D. Xiang and G. Stupakov, Echo-enabled harmonic generation free electron laser, Phys. Rev. ST Accel. Beams **12**, 030702 (2009).

[11] E. Hemsing, M. Dunning, B. Garcia, C. Hast, T. Raubenheimer, G. Stupakov, and D. Xiang, Echo-enabled harmonics up to the 75th order from precisely tailored electron beams, Nat. Photonics **10**, 512 (2016).

[12] P. Rebernik Ribič, A. Abrami, L. Badano, M. Bossi, H.-H. Braun, N. Bruchon, F. Capotondi, D. Castronovo, M. Cautero, P. Cinquegrana *et al.*, Coherent soft X-ray pulses from an echo-enabled harmonic generation free-electron laser, Nat. Photonics **13**, 555 (2019).

[13] E. Hemsing, A. Marinelli, G. Marcus, and D. Xiang, Correlated energy-spread removal with space charge for high-harmonic generation, Phys. Rev. Lett. **113**, 134802 (2014).

[14] S. Khan, G. Perosa, F. Sottocorona, E. Allaria, A. Brynes, G. Penco, P. R. Ribič, S. Spampinati, C. Spezzani, M. Trovò *et al.*, Evolution of microbunching in drift sections, in *Proceedings of the 40th International Free-Electron Laser Conference, IPAC-2022, Trieste, Italy* (JACoW, Geneva, Switzerland, 2022), pp. 21–24, 10.18429/JACoW-FEL2022-MOP01.

[15] S. Khan, G. Perosa, F. Sottocorona, E. Allaria, A. Brynes, G. Penco, P. R. Ribič, S. Spampinati, C. Spezzani, M. Trovò *et al.*, Space charge effects on density-modulated electron beams in drift spaces, in Proceedings of the 14th International Particle Accelerator Conference, IPAC-2023, Venice, Italy (JACoW, Geneva, Switzerland, 2023), pp. 1835–1838, 10.18429/JACoW-IPAC2023-TUPL033.

[16] E. Allaria, L. Badano, S. Bassanese, F. Capotondi, D. Castronovo, P. Cinquegrana, M. B. Danailov, G. D'Auria, A. Demidovich, R. De Monte *et al.*, The FERMI free-electron lasers, J. Synchrotron Radiat. **22**, 485 (2015).

[17] E. Allaria, R. Appio, L. Badano, W. A. Barletta, S. Bassanese, S. G. Biedron, A. Borga, E. Busetto, D. Castronovo, P. Cinquegrana *et al.*, Highly coherent and stable pulses from the FERMI seeded free-electron laser in the extreme ultraviolet, Nat. Photonics **6**, 699 (2012).

[18] C. Spezzani, E. Allaria, L. Badano, D. Castronovo, P. Cinquegrana, M. B. Danailov, R. De Monte, G. De Ninno, P. Delgiusto, A. Demidovich *et al.*, FERMI FEL-1 upgrade to EEHG, in *Proceedings of the 13th International Particle*

Accelerator Conference, IPAC'22, Bangkok, Thailand (JACoW, Geneva, Switzerland, 2022), pp. 1044–1046, 10.18429/JACoW-IPAC2022-TUPOPT019.

[19] E. Allaria, D. Castronovo, P. Cinquegrana, P. Craievich, M. Dal Forno, M. B. Danailov, G. D'Auria, A. Demidovich, G. De Ninno, S. Di Mitri *et al.*, Two-stage seeded soft-X-ray free-electron laser, Nat. Photonics **7**, 913 (2013).

[20] E. Allaria, L. Badano, F. Bencivenga, C. Callegari, F. Capotondi, D. Castronovo, P. Cinquegrana, M. Coreno, M. B. Danailov, A. Demidovich *et al.*, Future upgrade strategy for the FERMI seeded FEL facility, in *Proceedings of the 40th Free-Electron Laser Conference, FEL-2022, Trieste, Italy* (JACoW, Geneva, Switzerland, 2022), pp. 272–275, 10.18429/JACoW-FEL2022-TUP53.

[21] K. Hacker, R. Molo, S. Khan, L. L. Lazzarino, C. Lechner, Th. Maltezopoulos, T. Plath, J. Rossbach, S. Ackermann, J. Bödewadt *et al.*, Measurements and simulations of seeded electron microbunches with collective effects, Phys. Rev. ST Accel. Beams **18**, 090704 (2015).

[22] M. Zangrando, A. Abrami, D. Bacescu, I. Cudin, C. Fava, F. Frassetto, A. Galimberti, R. Godnig, D. Giuressi, L. Poletto *et al.*, The photon analysis, delivery, and reduction system at the FERMI@Elettra free electron laser user facility, Rev. Sci. Instrum. **80**, 113110 (2009).

[23] C. Svetina, D. Cocco, N. Mahne, L. Raimondi, E. Ferrari, and M. Zanggrando, PRESTO, the on-line photon energy spectrometer at FERMI: Design, features and commissioning results, J. Synchrotron Radiat. **23**, 35 (2016).

[24] M. Veronese, R. Appio, P. Craievich, and G. Penco, Absolute bunch length measurement using coherent diffraction radiation, Phys. Rev. Lett. **110**, 074802 (2013).

[25] M. Ferianis, E. Allaria, E. Ferrari, G. Gaio, G. Penco, F. Rossi, and M. Veronese, How the optical timing system, the longitudinal diagnostics and the associated feedback systems provide femtosecond stable operation at the FERMI free electron laser, High Power Laser Sci. Eng. **4**, e13 (2016).

[26] K. Hacker, Longitudinal space charge assisted echo seeding of a free-electron laser with laser-spoiler noise suppression, Phys. Rev. ST Accel. Beams **17**, 090702 (2014).

[27] Y. Liang, Z. Liu, Q. Tian, T. Li, X. Lin, L. Yan, Y. Du, R. Li, J. Shi, C. Cheng *et al.*, Widely tunable electron bunch trains for the generation of high-power narrowband 1–10 THz radiation, Nat. Photonics **17**, 259 (2023).

[28] J. Yan, Z. Gao, Z. Qi, K. Zhang, K. Zhou, T. Liu, S. Chen, C. Feng, C. Li, L. Feng *et al.*, Self-amplification of coherent energy modulation in seeded free-electron lasers, Phys. Rev. Lett. **126**, 084801 (2021).

[29] G. Paraskaki, E. Allaria, E. Schneidmiller, and W. Hillert, High repetition rate seeded free electron laser with an optical klystron in high-gain harmonic generation, Phys. Rev. Accel. Beams **24**, 120701 (2021).